Test and Modelling of Impact on Pre-Loaded Composite Panels

A. K. Pickett · M. R. C. Fouinneteau · P. Middendorf

Abstract Currently test and simulation of low and high speed impact of Aerospace composite structures is undertaken in an unloaded state. In reality this may not be the case and significant internal stresses could be present during an impact event such as bird strike during landing, or takeoff. In order to investigate the effects of internal loading on damage and failure of composite materials a series of experimental and simulation studies have been undertaken on three composite types having different fibres, resins and lay-ups. For each composite type panels have been manufactured and transversely impacted under the condition of 'unloading' or 'pre-loading'. For preloading a rig has been constructed that can impose a constant in plane strain of up to 0.25% prior to impact. Results have clearly shown that preloading does lower the composite impact tolerance and change the observed failure modes. Simulation of experiments have also been conducted and have provided an encouraging agreement with test results in terms of both impact force time histories and prediction of the observed failure mechanisms.

Nomenclature

Symbol	Meaning	Units
QI	Quasi Isotropic	
E_{11}^t	Tensile Young's modulus in the 1-direction	GPa

A. K. Pickett (✉)
Institute for Aircraft Design, University of Stuttgart, Stuttgart, Germany
e-mail: tony.pickett@arcor.de

M. R. C. Fouinneteau
School of Applied Science, Cranfield University, Bedfordshire, UK

P. Middendorf
EADS, Ottobrunn, Germany

E_{11}^{c}	Compressive Young's modulus in the 1-direction	GPa
E_{22}^{t}	Tensile Young's modulus in the 2-direction	GPa
G_{12}	Shear modulus in the 1,2 plane	GPa
G_{23}	Shear modulus in the 2,3 plane	GPa
v_{12}^{0}	Poisson's ratio in 1,2-plane	-
Y_{12C}	Critical shear damage limit	√GPa
Y_{120}	Initial shear damage limit	√GPa
$Y_{22C}^{'}$	Critical transverse damage limit	√GPa
$Y_{220}^{'}$	Initial transverse damage limit	√GPa
b	Coupling factor between shear and transverse damage	
$Y_{22S}^{'}$	Transverse damage limit for matrix cracking	√GPa
Y_{12R}	Shear damage limit of fibre-matrix interface	√GPa
d_{max}	Maximum shear damage	-
ε_{11i}^{t}	Tensile fibre initial strain	-
ε_{llu}^{c}	Tensile fibre ultimate strain	-
d_{11u}^{t}	Tensile fibre ultimate damage	-
γ	Compressive factor for non-linear fibre compressive behaviour	-
ε_{11i}^{c}	Compressive fibre initial strain	-
ε_{11u}^{c}	Compressive fibre ultimate strain	-
d_{11u}^{c}	Compressive fibre ultimate damage	-
β	Hardening law multiplier	GPa
α	Hardening law exponent	-
R_{0}	Initial yield stress	GPa
a^{2}	Coupling factor between shear and transverse plastic strains	-

1 Introduction

Carbon fibre composites are being increasingly used in the aerospace industry to replace aluminium alloys due to advantages of high specific stiffness and strength, good corrosion resistance and fatigue characteristics. However, composites are more difficult to character-ise than isotropic materials, especially if properties such as failure under static and dynamic loading are considered. In aircraft structures an important design consideration is performance of the structure due to low or high velocity impact from events such as 'tool drop' and debris or bird strike, and tests are routinely conducted by manufacturers to assess material and structure performance subject to such impact cases.

Standardised tests, for example the ASTM standards [1] and [2], are available to assess the damage resistance and residual compressive strength of a composite following a drop weight impact event. This test is performed at relatively low energies using a small, low velocity impactor that leaves a barely visible indent; post impact testing of the specimen investigates the change in in-plane compression strength due to any impact damage. These impact conditions are considerably different to the experimental and simulation studies undertaken in this paper which attempt to evaluate damage in composites subjected to significant impact energy. Furthermore, additional pre-loading is imposed which is intended

to more closely reproduce the likely loading conditions in an aircraft structure during a real impact event.

Only limited work appears in the open literature concerning the effect on pre-straining of composites during impact loading. Whittingham et al. [3] presented a combined tensile/compressive panel which was simultaneously impacted with a 12 mm spherical impactor having relatively low levels of energy (between 6 J to 10 J). These results found that the nature and magnitude of pre-straining did not affect the penetration/perforation depth, or the peak load and absorbed energy. The effect of pre-staining has also been investigated numerically by Mikkor et al. [4] using the explicit FE code PAM-CRASH[TM] [5]; however, this work did not consider delamination as a potential failure mode and used a so-called Bi-Phase ply composites model that has limited capabilities to treat transverse matrix and shear failure. Various parameters such as preload magnitude, impact velocity and impact specimen geometry were investigated to study the damage incurred and residual strength; in this work significant changes to the failure behaviour were observed and shown to be dependent on the magnitude of pre-loading.

The work presented in this paper considers three laminate types having either a quasi-isotropic, or ±45º lay-up, and two different fibre-resin material systems. The experimental work includes an extensive materials characterisation program to determine material parameters for the constitutive laws to be used in the numerical models. The rig design and methodology used to introduce the uni-axial pre-loading are also presented together with experimental results for unloaded and pre-loaded composite panels subjected to significant impact loading. Numerical modelling of the composite laminate uses an elasto-plastic with damage model for each ply, and a delamination interface between plies, so that all principal composites failure mechanisms are represented; thus the modelling approach should be a significant advance to the work reported by Mikkor et al. [4]. Numerical simulations of the loaded and unloaded panels are undertaken and comparisons made with tests. Both the experimental and simulation results have found that damage and failure mechanisms are dependent of the level of pre-loading applied to the plate prior to impact.

2 The Materials and Composite Lay-Ups Investigated

For this work composite panels have been investigated using two different composite materials systems; namely, a high performance Aerospace unidirectional prepreg (T800S/M21) manufactured in an autoclave and a biaxial Non Crimp Fabric (NCF) with two part infused epoxy resin (NCF/LY3505) manufactured using the VARI process. Details of the two materials are given in Table 1. For each material the manufacturers processing and curing recommendations were followed. Details of the composite panel materials, lay-ups and thicknesses are given in Table 2.

Table 1 Material specifications for T800S/M21 and NCF/LY3505

Material type	Prepreg/Fabric	Resin
Material 1 - (T800S/M21): M21/35%/268/T800S Pre-impregnated and cured in Autoclave	Unidirectional [0°] Area weight: 412 g/m² Manufacturer: Hexcel	Epoxy resin: M21 Manufacturer: Hexcel
Material 2 - (NCF/LY3505): NCF/LY3505 - Dry fabric infused using the VARI process and post cured	Biaxial [±45°] Fibre: Tenax HTA carbon Area weight: 540 g/m² Tow grade: 6 k Manufacturer: Saertex	Epoxy resin: LY3505 Hardener: XB3403 Manufacturer: Huntsman

Table 2 Composite panels specifications

Composite panel	Material	Lay-up	Thickness
Study 1a (unloaded) Study 1b (pre-loaded)	T800S/M21	[0/90,±45,0/90,±45, 0/90,±45,0/90,±45]$_S$	4.3 mm
Study 2a (unloaded) Study 2b (pre-loaded)	NCF/LY3505	[0/90,±45,0/90,±45,0/90,±45, 0/90,±45]$_S$	4.2 mm
Study 3a (unloaded) Study 3b (pre-loaded)	NCF/LY3505	[±45]$_{16}$	4.2 mm

3 The Composite Ply and Delamination Damage Models

### 3.1 The Meso-Scale Ply Damage Model

Evolution of damage in composites has been studied at both the micro– (fibre and matrix) and meso-scale (individual layer) levels. Amongst numerous damage theories applied to composites the meso-scale uni-directional ply damage model proposed by Ladevèze and Le Dantec [6] has demonstrated success for damage and failure prediction. This model, with minor adaptations, has also been successfully applied to NCF carbon/epoxy composites [7] and carbon/glass braided composites [8, 9] where large fibre re-orientations are involved. This model considers the laminate to be constructed from elementary unidirectional plies, Fig. 1, with each ply having a constant thickness and fibres running in one principal direction. A state of plane stress is assumed and subscripts 1, 2 and 3 denote the fibre, transverse and through thickness directions respectively.

This model has been implemented in a multi-layered thin shell element in the explicit Finite Element code PAM-CRASH^{TM}. This allows each ply in the laminate to be represented using an orthotropic elasto-plastic with damage stress-strain relationship given by,

$$\varepsilon^e = S\sigma \tag{1}$$

The stress and strain vectors are,

$$\begin{aligned}
\{\sigma\} &= \{\ \sigma_{11} \quad \sigma_{22} \quad \sigma_{12}\ \}^T \\
\{\varepsilon^e\} &= \{\ \varepsilon_{11}^e \quad \varepsilon_{22}^e \quad 2\varepsilon_{12}^e\ \}^T
\end{aligned} \tag{2}$$
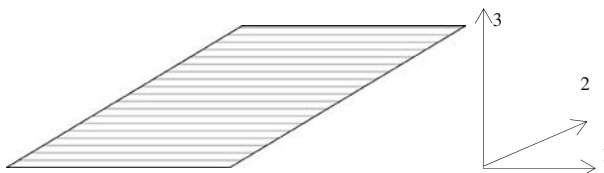
Fig. 1 Elementary 'equivalent' unidirectional ply [6]

and the stiffness matrix $[S]$ has the following form and coefficients,

$$[S] = \begin{bmatrix} 1/E_{11}^0 & -v_{12}^0/E_{11}^0 & 0 \\ -v_{12}^0/E_{11}^0 & 1/E_{22}^0(1-d_{22}) & 0 \\ 0 & 0 & 1/G_{12}^0(1-d_{12}) \end{bmatrix} \tag{3}$$

where ε^e and superscript ^{0} are the elastic strain and undamaged values respectively. E_{11}^0 and E_{22}^0 are elastic modulii in the fibre and transverse directions, G_{ij}^0 is shear modulus and v_{ij}^0 is Poisson's ratio. Matrix damage in the transverse and shear directions is given by d_{22} and d_{12}.

For fibre failure (direction 11) a simple maximum strain criteria is used to control the initiation and ultimate strain to failure. For tension these are parameters ε^t_{11i} and ε^c_{11u}, and for compression ε^c_{11i} and ε^c_{11u}, with values determines from tension and compression coupon tests. In tension the stress-strain response is linear to failure, whereas in compression crimp and fibre microbuckling can lead to a nonlinear response that is approximated by the scalar corrective parameter γ,

$$E_{11}^{\gamma c} = \frac{E_{11}^{0c}}{1 + \gamma E_{11}^{0c}|\varepsilon_{11}^c|} \tag{4}$$

where $\gamma = \frac{E_{11}^{0c} - E_{11}^{\gamma c}}{E_{11}^{\gamma c} E_{11}^{0c}|\varepsilon_{11}^\gamma|}$

and E^{0c}_{11} and $E^{\gamma c}_{11}$ are the initial and reduced compressive modulus at an arbitrarily selected compressive stress $\varepsilon^{\gamma c}_{11}$. Fibre damage d_{11} varies linearly from zero (no damage) to one (full damage) between the following limits,

$$\begin{array}{ll} \text{in tension} & \varepsilon^t_{11i} \leq \varepsilon^t_{11} \leq \varepsilon^t_{11u} \\ \text{in compression} & \varepsilon^c_{11i} \geq \varepsilon^c_{11} \geq \varepsilon^c_{11u}. \end{array} \tag{5}$$

Matrix transverse and shear damage are controlled by the variables d_{22} and d_{12}, which vary from 0 (no damage) to 1.0 (fully damaged), and measure loss in transverse and shear modulii stiffness respectively. Therefore, at any instant the damaged modulii E_{22}^D and G_{12}^D are given by the relations,

$$\begin{array}{l} E_{22}^D = E_{22}^0(1-d_{22}) \\ G_{12}^D = G_{12}^0(1-d_{12}). \end{array} \tag{6}$$

The damage functions (d_{22} and d_{12}) are associated with conjugate quantities Y_{22} and Y_{12} respectively, which govern damage development. These quantities are partial derivatives of the damaged material strain energy,

$$\begin{aligned} E_D &= \tfrac{1}{2}\underline{\underline{\sigma}} : \underline{\underline{\varepsilon}}^e, \\ &= \frac{1}{2}\left[\frac{(\sigma_{11})^2}{E_{11}^0} - 2\frac{v_{12}^0}{E_{11}^0}\sigma_{11}\sigma_{22} + \frac{\langle\sigma_{22}^e\rangle_+^2}{E_{22}^0(1-d_{22})} + \frac{\langle\sigma_{22}^e\rangle_-^2}{E_{22}^0} + \frac{\sigma_{12}^e{}^2}{G_{12}^0(1-d_{12})} \right] \end{aligned} \tag{7}$$

with

$$\begin{array}{ll} \langle x \rangle_+ = x & \text{if } x > 0, \quad \text{otherwise } \langle x \rangle_+ = 0 \\ \langle x \rangle_- = x & \text{if } x < 0, \quad \text{otherwise } \langle x \rangle_- = 0 \ . \end{array}$$

The expressions for Y_{12} and Y_{22} are,

$$
\begin{aligned}
Y_{12} &= -\frac{\partial E_D}{\partial d_{12}} = \frac{\sigma_{12}^2}{2G_{12}^0(1-d_{12})^2} \\
Y_{22} &= -\frac{\partial E_D}{\partial d_{22}} = \frac{\sigma_{22}^2}{2E_{22}^0(1-d_{22})^2}.
\end{aligned}
\tag{8}
$$

Equations [8] govern damage evolution and are analogous to strain energy release rates governing crack propagation. The relationships between damages $\{d_{22}, d_{12}\}$ and conjugate quantities $\{Y_{22}, Y_{12}\}$ is usually interpolated using a linear form such as,

$$
\begin{cases}
d_{22} = h(Y_{22}) = \frac{Y_{22}-Y_{220}}{Y_{22C}} & \text{if } d_{22} < 1, \quad otherwise \ d_{22} = 1 \\
\\
d_{12} = g(Y_{12}) = \frac{Y_{12}-Y_{120}}{Y_{12C}} & \text{if } d_{12} < 1, \quad otherwise \ d_{12} = 1 ,
\end{cases}
\tag{9}
$$

where Y_{220}, Y_{22c}, Y_{120}, and Y_{12c} are material constants.

Damage interaction is introduced by the coupling parameter b, which is generally determined from experiments, leading to the final governing equation for coupled transverse-shear damage,

$$
\overline{Y}(t) = \sup_{r \leq t}\left(\sqrt{Y_{12}(\tau) + bY_{22}(\tau)}\right)
\tag{10}
$$

A cyclic tensile coupon test of a $[\pm 45°]$ laminate is used to characterise matrix shear damage and plasticity evolution. The global laminate stresses and strains are transformed to assess the local ply shear stress-strain curve, see for example Fig. 2, where the degradation of the ply shear modulus $G_{12,i}$ and the generation of inelastic ply deformation $2\varepsilon_{12,i}^p$ can be clearly observed.

The plasticity model proposed by Ladevèze and Le Dantec for UD composites has been found appropriate and is used here. In order to couple damage and plasticity, effective stress $\widetilde{\sigma}_{ij}$ and effective plastic strains $\dot{\widetilde{\varepsilon}}_{ij}^p$ are introduced as follows,

$$
\begin{aligned}
\widetilde{\sigma}_{ij} &= \begin{bmatrix} \widetilde{\sigma}_{11} \\ \widetilde{\sigma}_{22} \\ \widetilde{\sigma}_{12} \end{bmatrix} = \begin{bmatrix} \sigma_{11} \\ [\langle\sigma_{22}\rangle_+/(1-d_{22})] + \langle\sigma_{22}\rangle_- \\ \sigma_{12}/(1-d_{12}) \end{bmatrix} \\
\dot{\widetilde{\varepsilon}}_{ij}^p &= \begin{bmatrix} \dot{\widetilde{\varepsilon}}_{11}^p \\ \dot{\widetilde{\varepsilon}}_{22}^p \\ \dot{\widetilde{\varepsilon}}_{12}^p \end{bmatrix} = \begin{bmatrix} 0 \\ (\dot{\varepsilon}_{22}^p/\sigma_{22})[\langle\sigma_{22}\rangle_+(1-d_{22}) + \langle\sigma_{22}\rangle_-] \\ \dot{\varepsilon}_{12}^p(1-d_{12}) \end{bmatrix} .
\end{aligned}
\tag{11}
$$

Assuming isotropic hardening and that plastic strains are independent of σ_{11} the elasticity domain is given by the yielding function f as,

$$
f(\widetilde{\sigma}, R) = \sqrt{\widetilde{\sigma}_{12}^2 + a^2\widetilde{\sigma}_{22}^2} - R(\widetilde{p}) - R_0 ,
\tag{12}
$$
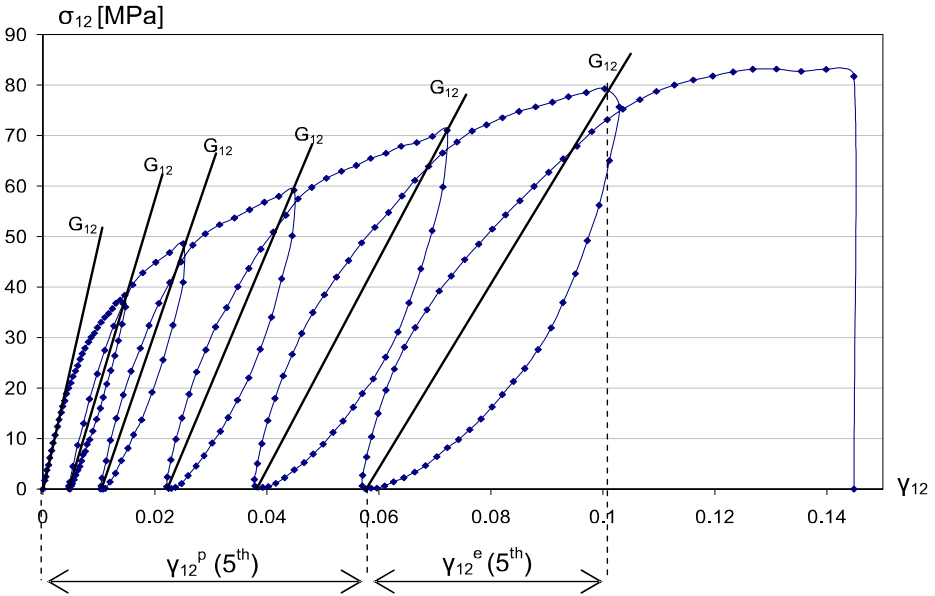
Fig. 2 Procedure and cyclic shear test for damage and plasticity determination of composite NCF/LY3505

where R_0 and $R(\tilde{p})$ are the initial yielding stress and a hardening function expressed in terms of accumulated plastic strain $\tilde{p}$. The factor a^2 accounts for material anisotropy. Assuming an isotropic matrix material it can be shown from the 'Von Mises' yield condition that $a^2 = 1/3$. A power law is assumed for plastic strain hardening,

$$R(p) = \beta p^\alpha, \qquad (13)$$

where β and α are curve fitting parameters. The equivalent plastic strain p is given by,

$$p = \int_0^{\varepsilon_{12}^p} 2\left(1 - d_{12}\right) d\varepsilon_{12}^p, \qquad (14)$$

where the plastic shear strain increment $d2\varepsilon_{12}^p$ is the difference between the total and elastic shear strain increments,

$$d2\varepsilon_{12}^p = d2\varepsilon_{12}^t - d2\varepsilon_{12}^e \qquad (15)$$

3.2 The Interface Delamination Model

The cohesive crack model proposed by Hillerborg et al. [10] has been applied by Pickett et al., and others, for composites delamination modelling, see for example [11, 12]. The approach adopted is to tie shell (or solid) finite element layers together with a mechanical

stiffness-damage law that represents elastic, failure and energy absorption of the resin interface during loading, crack initiation and crack growth (delamination). Fig. 3 shows the attachment of two surfaces; arbitrarily called the slave and master surfaces. At initialisation each slave node on a slave surface is attached to a fictitious 'shadow' node created on the adjacent master surface (element). During deformation the relative movement of the slave and shadow node provides the normal and shear deformations that are used in the mechanical laws to compute the elastic-damaging normal and shear resisting forces.

The main features of the interface mechanical law are shown in Fig. 3b for normal Mode I loading. A simple linear elastic law is assumed up to the failure stress σ_{Imax}. Thereafter, linear damaging is activated so that at final separation δ_{Imax} the fracture energy of the tied interface has been absorbed. The area under the curve corresponds to the critical energy release rate G_{Ic} generated in creating the fracture surface. Thus σ_{Imax}, δ_{Ic} and δ_{Imax} are selected so that the elastic-damage curve fulfils the required criteria. Identical arguments are used to define the shear (Mode II) curve.

The following formulae describe Mode I failure; identical equations are used for Mode II by interchanging E_0, σ_{Imax}, δ_I and G_{Ic} with G_0, σ_{IImax}, δ_{II} and G_{IIc}. The through thickness normal modulus E_0 relates stress to displacement for the composite inter-ply interface in the elastic region. At the maximum normal stress σ_{Imax} damage is initiated and the stress displacement law then follows a linear damage equation of the type,

$$\sigma_I = (1 - d_I) \cdot E_0 \cdot \varepsilon_I = (1 - d_I) \cdot E_0 \cdot \frac{\delta_I}{L_0}, \qquad (16)$$

where d_I is the damage parameter that varies between 0 (undamaged) and 1 (fully damaged), E_0 is the modulus, L_0 the normal distance between the original position of the slave node and the master element and δ_I the deformed normal separation distance of the slave node and master element. The area under the stress-displacement curve in the elastic range G_{IA} is the fracture energy required to initiate damage and is given by,

$$G_{IA} = \frac{1}{2} \frac{\sigma_{Imax}^2}{E_0} L_0. \qquad (17)$$
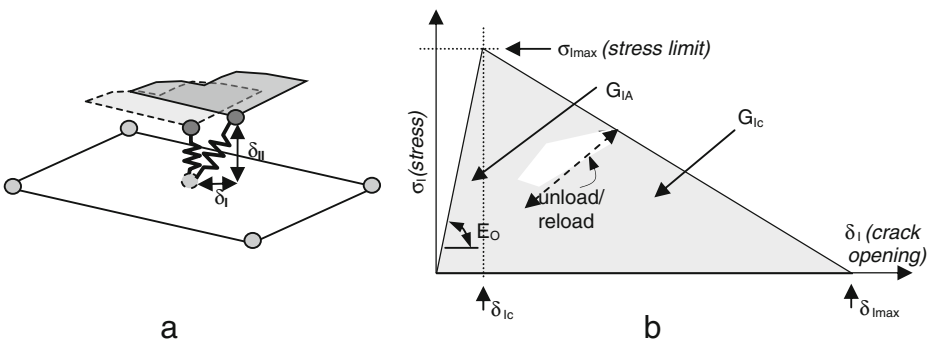
Fig. 3 The inter-ply delamination model, **a** an attached node (adjacent 'slave' node) constrained to an element 'master' surface, **b** Diagram of the stress-crack opening curve for Mode I loading

The total area under the load-displacement curve is the critical energy release rate required for failure of the interface and is given by,

$$G_{Ic} = \frac{1}{2}\sigma_{\mathrm{I}max}\delta_{\mathrm{I}max}. \tag{18}$$

The values of G_{Ic} and G_{IIc} and other model parameters can be obtained via the standard Double Cantilever Beam (DCB) test [13] and End Notched Flexure (ENF) test [14]. In real materials there is a coupling between normal and shear loading and the critical energy release rate. This interaction can be determined using the Mixed Mode Bending (MMB) test [15] to provide the coupling parameter α used in the following mixed mode interaction model,

$$\left(\frac{G_I}{G_{In}}\right)^{\alpha} + \left(\frac{G_{II}}{G_{IIn}}\right)^{\alpha} = 1, \tag{19}$$

where n = A for the onset of fracture and n = C for fracture; G_I and G_{II} are the instantaneous values and G_{In} and G_{IIn} are test values as measured by the DCB and ENF tests. Example solutions using this approach, including validation against DCB, ENF and MMB tests have been presented for composite delamination modelling [16]. In this work a linear interaction model ($\alpha=1$) has been assumed.

4 Materials Characterisation

4.1 Ply Testing and the Ply Damage Model

The ply damage model defines orthotropic elasticity, damage and plasticity for a unidirectional elementary ply. The original test program is specific to UD laminates and involves tension, compression and cyclic tension-shear tests on a variety of laminates including $[0°]_8$, $[\pm 45°]_{2S}$, $[\pm 67.5°]_{2S}$ and $[+45°]_8$ lay-ups to determine the constitutive elastic, damage and plasticity properties. Full details of the test program and parameter identification are to be found in [5, 6].

For the T800S/M21 ply data this testing program was undertaken [17] giving the data reproduced in Table 3. For the biaxial NCF/LY3505 the test program and model must be necessarily adapted for bi-axial fabrics and the impossibility to test individual UD layers; furthermore, some tests become irrelevant due to the different failure mechanisms that occur. Tension and compression testing to failure is straightforward and used the conventional ASTM standard tests on $[0°/90°]$ coupons to obtain elastic and failure data. Shear testing used a $[\pm 45°]$ coupon cyclic loaded in tension, from which the σ_{12} versus ε_{12} curve may be obtained, Fig. 2. The shear modulus $G_{12}{}^i$ for each cycle is calculated from elastic strain $\gamma_{12}{}^{ie}$ and the corresponding shear stress $\sigma_{12}{}^{ip}$. In addition, in order to monitor the evolution of plasticity, plastic strains $\gamma_{12}{}^{ip}$ are extracted for each cycle. At least 5–6 cycles are required to obtain a good evolution of damage and plasticity. Classical laminate analysis was used to define an equivalent 'NCF' unidirectional ply. This method of determination can be found in greater detail in [9]. Table 4 gives the elastic properties and fibre damage parameters for the NCF/LY3505 material.

Table 3 Properties for a T800S/M21 ply

Elastic properties

	$E_{11}^{t0}=E_{11}^{c0}$ (GPa)	v_{12}^0	E_{22}^0 (GPa)	G_{12}^0 (GPa)	G_{23}^0 (GPa)		
	179.0	0.37	10.0	7.02	7.02		

Fibre damage parameters

	Tension			**Compression**			
	ε_{11i}^t	ε_{11u}^t	d_{11u}^t	γ	ε_{11i}^c	ε_{11u}^c	d_{11u}^c
	0.0125	0.0130	0.9	0.0001	0.0080	0.0085	0.9

Shear/Transverse damage law

Y_C ($\sqrt{GPa}$)	Y_0 ($\sqrt{GPa}$)	Y'_C ($\sqrt{GPa}$)	Y'_0 ($\sqrt{GPa}$)	b	Y'_S ($\sqrt{GPa}$)	Y_R ($\sqrt{GPa}$)	d_{max}
0.079	0.0001	0.0725	0.010	1.5	0.016	0.065	0.9

Plasticity law $R(p) = \beta p^\alpha$

	R_0 (GPa)	β (GPa)	α
	0.010	0.87	0.61

4.2 Delamination Testing and the Delamination Model

Data for the delamination model of the two composite material systems are presented in Table 5. For the T800S/M21 material DCB testing was used to determine G_{IC}, from which a simulation model of the DCB test was used to calibrate the remaining Mode I parameters (σ_I^{prop} and E_0) against test measurements [17]; the Mode II parameters have been estimated. For the NCF/LY3505 material a full test program using DCB and ENF testing has been conducted [16] to obtain the parameters presented in Table 5; in this case only the pure Mode I and pure Mode II values, GIc and GIIc respectively, have been used and a linear interaction model with $\alpha=1$ in Equation 19 was assumed.

Table 4 Properties for an 'equivalent' NCF/LY3505 ply

Elastic properties

	$E_{11}^{t0}=E_{11}^{c0}$ (GPa)	v_{12}^0	E_{22}^0 (GPa)	G_{12}^0 (GPa)	G_{23}^0 (GPa)		
	127.8	0.30	7.127	4.85	4.85		

Fibre damage parameters

	Tension			**Compression**			
	ε_{11i}^t	ε_{11u}^t	d_{11u}^t	γ	ε_{11i}^c	ε_{11i}^c	d_{11u}^c
	0.0132	0.0132	0.9	0.1	0.0080	0.0081	0.9

Shear/Transverse damage law

Y_C ($\sqrt{GPa}$)	Y_0 ($\sqrt{GPa}$)	Y'_C ($\sqrt{GPa}$)	Y'_0 ($\sqrt{GPa}$)	b	Y'_S ($\sqrt{GPa}$)	Y_R ($\sqrt{GPa}$)	d_{max}
0.0668	0.0049	10E06	10E-6	2.7	10.0	0.0667	0.9

Plasticity law $R(p) = \beta p^\alpha$

	R_0 (GPa)	β (GPa)	α
	0.017	0.934	0.586

Table 5 Parameters for the delamination interface model for materials T800S/M21 and NCF/LY3505

Parameters	Notation	T800S/M21	NCF/LY3505
Distance for kinematics computation (mm)	h_{cont}	0.5	0.5
Normal modulus (GPa)	E_0	5.0	7.8
Shear modulus (GPa)	G_0	2.5[*]	2.5[*]
Normal propagation stress (GPa)	σ_I^{prop}	0.020[*]	0.020
Shear propagation stress for delamination (GPa)	σ_{II}^{prop}	0.030[*]	0.030
Mode I fracture Energy for delamination (J/mm^2)	G_{IC}	0.63E-03	0.47E-03
Mode II fracture Energy for delamination (J/mm^2)	G_{IIC}	2.70E-03[*]	2.00E-03

[*] estimated parameters

5 Impact Testing

5.1 Test Setup and Procedures

Pre-straining of the composite panels used a purpose built loading rig, Fig. 4. Briefly, the rig comprises of two stiff frames that are placed above and below the composite test panel. Each composite panel was 600 mm long by *200 mm wide and had 50 mm aluminium tabs bonded to the ends for good load introduction. This panel size represented a practical maximum size that could be tested in the drop tower facility. Loading blocks were attached to the tabs via 10 bolts; the loading blocks were connected to the outer frame by 4 regular spaced bolts which imposed the required pre-loading. A simple 10 mm wide support is provided lengthwise under each of the sides to provide lateral support and limit out of plane deformations during transverse impact.

　　In order to check a uniform state of strain exists in the panel the rig was first tested using a pre-loaded steel sheet having several strain gauges distributed over the surface.
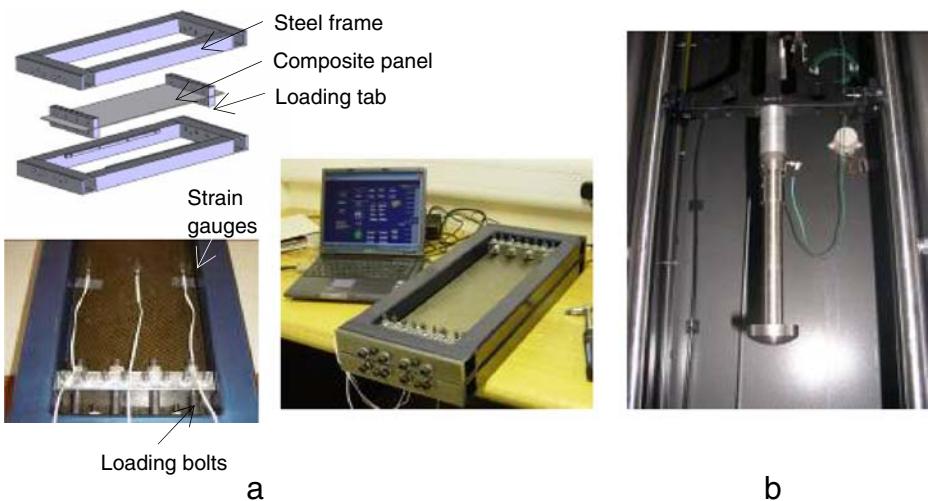
Fig. 4 The rig and test set up to impact composite plates; **a** the loading frame and calibration, **b** the 50 mm diameter impactor

Furthermore, the steel sheet of known Young's modulus (210 GPa) was used to calibrate the system by correlating applied bolt torque to strain (and stress) in the calibration plate. Thus applied bolt torque can then be used to impose a specific pre-loading, or specific pre-strain to the composite plate provided Young's modulus for the plate is known in the loading direction.

For the pre-loaded panels a moderate pre-strain of 0.25% was selected and used throughout this work; this pre-strain represented a practical limit for the rig and is close to the usual limit design limit strains of 0.3–0.4% used for Aerospace composites. The rig, with the unloaded or pre-loaded panels, was placed inside a drop tower and impacted with a 50 mm diameter steel impactor having a mass of 21.1 kg and impact velocity of 5.77 m/s giving a total impact energy of 350 J. This impact energy was found to cause significant material damage for the selected composites and was an appropriate level to compare damage mechanisms for the different loading cases.

5.2 Test Results

Test results are presented for the different panels. Unfortunately the scope of the experimental program did not allow several specimens to be manufactured and tested for each composite type; consequently, in each case, only one panel per composite type was tested. Unfortunately, therefore, the degree scatter from this experimental work is unknown. Never-the-less it is felt that there are useful trends to be seen in the experimental and simulation results.
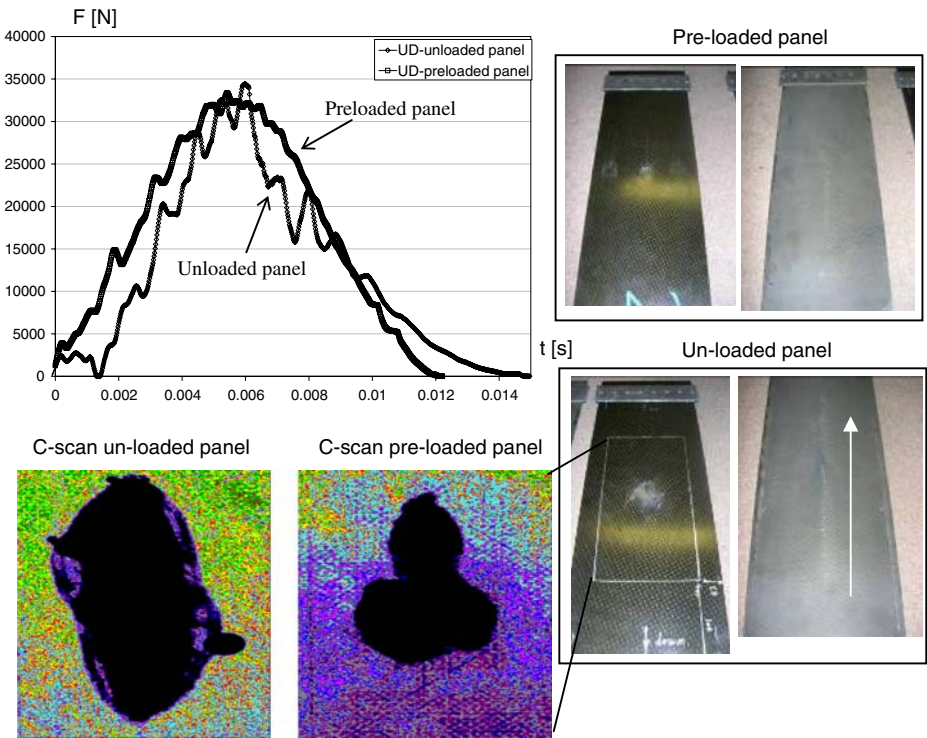
5.2.1 Studies 1a and 1b

Figure 5 shows test results for the unloaded and pre-loaded T800S/M21 quasi-isotropic panels, studies 1a and 1b respectively. The impact force time history shows that energy absorbed by the pre-loaded panel, as seen by the area under the force displacement curve, is higher; however, peaks loads reached for both cases are similar. Fibre damage is visually observed for both cases and C-scans reveal that approximately 50% more delamination occurs compared to the unloaded panel.
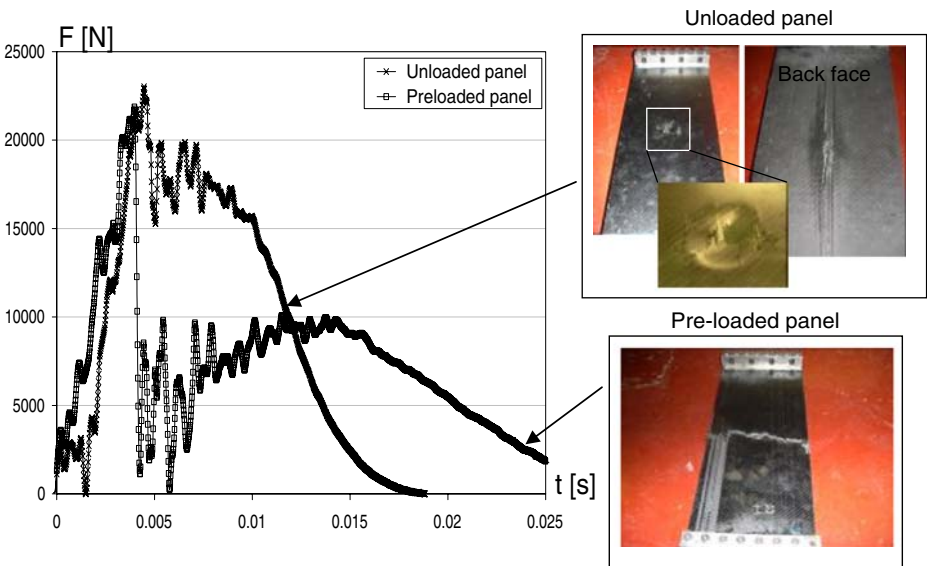
5.2.2 Studies 2a and 2b

Figure 6 shows test results for the unloaded and pre-loaded NCF/LY3505 quasi-isotropic panels, studies 2a and 2b respectively. The pre-strained panel exhibits a similar maximum load to the unloaded panel; however, in this case catastrophic failure does occur with a complete failure of the panel in the loading direction. After first failure the load rapidly drops off. The residual strength of the pre-loaded panel is due to the load bearing capacity in the width direction and the support from the lateral (side) supports. The unloaded panel undergoes significant damage to the top face under the punch and also exhibits longitudinal splitting on the lower face, but does withstand the impact loading without major failure.
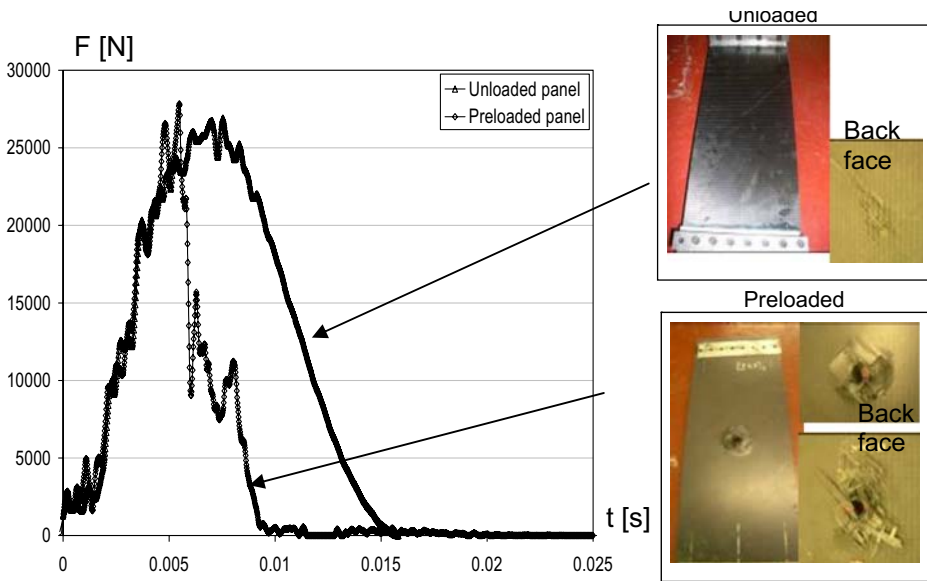
5.2.3 Studies 3a and 3b

Figure 7 shows test results for the unloaded and pre-loaded NCF/LY3505 $[\pm 45°]_{16}$ panels, studies 3a and 3b respectively. The maximum load for both cases is similar, except that the preloaded panel shows a sudden drop in load corresponding due to panel perforation. For the unloaded panel only minor internal damage and a barely visible indent has occurred.

Fig. 5 Studies 1a and 1b — Impact force versus time curves and failure mechanisms for the loaded and unloaded T800S/M21 QI panels

Fig. 6 Studies 2a and 2b — Impact force versus time curves and failure mechanisms for the loaded and unloaded NCF/LY3505 QI panels

Fig. 7 Studies 3a and 3b — Impact force versus time curves and failure mechanisms for the loaded and unloaded NCF/LY3505 [±45º]₁₆ panels

Clearly, in this case the preloading has loaded the fibre and matrix sufficiently such that during impact the superimposed loading causes major fibre and intra-ply shear failure mechanisms to occur.

6 Finite Element Modelling and Numerical Results

6.1 Simulation Model Setup

The explicit finite element code PAM-CRASH[TM] was used to simulate impact of the different unloaded and pre-loaded composite panels. Each panel is 600 mm long by 200 mm wide and for convenience a thickness of 4.2 mm was assumed for all laminates types. The FE model used 8 layers of shell elements, inter-connected by the delamination contact, to model the 16 plies; so that each multilayered shell element represents 2 plies, Fig. 8. The mesh used a regular element size of 10 mm*10 mm which is refined to 5 mm*5 mm under the punch where greatest deformation and damage occur.

The punch was modelled using rigid shell elements and assigned a mass of 21.1 kg and initial impact velocity of 5.66 m/sec. The rest bars were modelled using fully constrained solid elements. Both punch and rest bars were assigned contact definitions to the panel. Finally, the tabs and loading blocks where modelled using solid elements that were attached to the outer ply shell elements and either fully constrained, for the unloaded case, or given a velocity time history to pre-strain the panel prior to impacting with the punch, Fig. 8. For preloading the velocity time history, Fig. 9, is imposed at the loading tabs in both the positive and negative x-directions to give the required 0.25% pre-strain; the loading tabs are then held fixed and the punch impacts the plate at 5.66 m/sec.
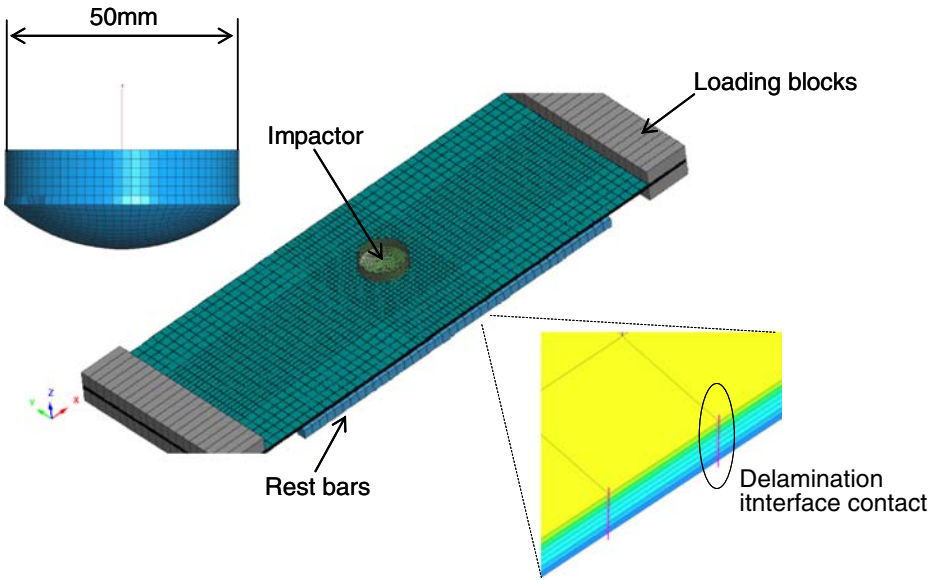
Fig. 8 The finite element model used to represent the impact problem

In total 6 simulations for studies 1a, 1b, 2a, 2b, 3a and 3b were undertaken. For the T800S/M21 and NCF/LY3505 materials the numerical models used appropriate data as specified in Tables 3 and 4, with delamination data as specified in Table 5.

6.2 Simulation Results and Comparison with Tests

Some general observations regarding the simulation results may be made for the three materials types considered with and without preloading. Simulation results for maximum ply damage (top ply), maximum ply damage (bottom ply) and an example of delamination
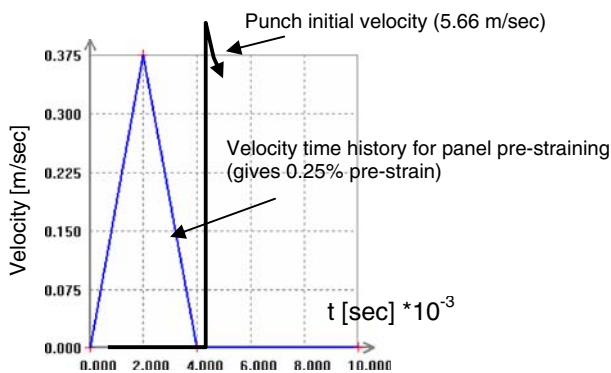
Fig. 9 Velocity time histories for loading the composite panels
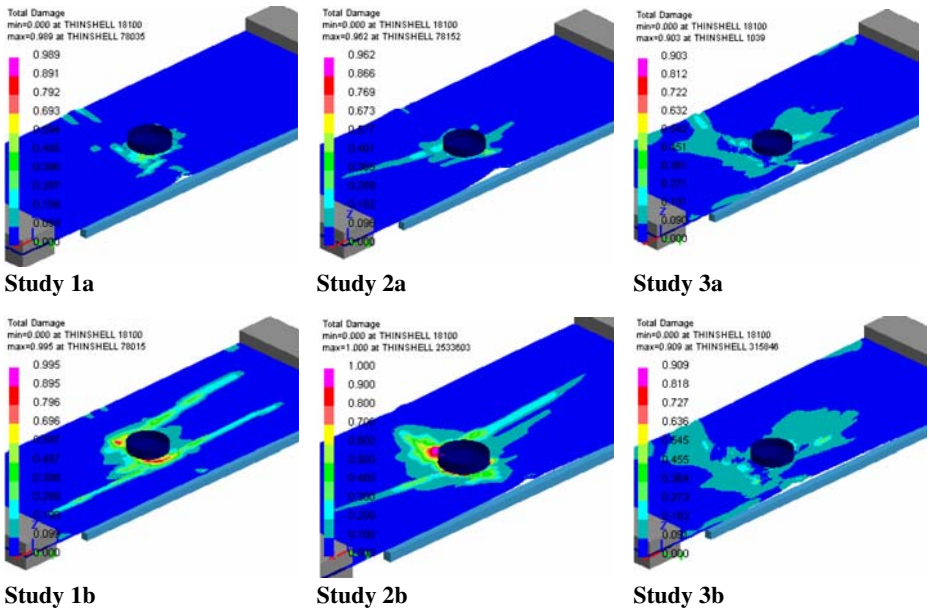
Fig. 10 Maximum ply damage on the upper ply (top view)

taken between the two central plies are shown in Figs. 10, 11 and 12, respectively, for the 6 case studies. In the damage plots "total damage" is the maximum of d11 (fibre), d22 (transverse) and d12 (shear) damage, as given by Equations 5 and 9, having contours that vary from zero (no damage) to one (full damage). In all cases there is a significant growth
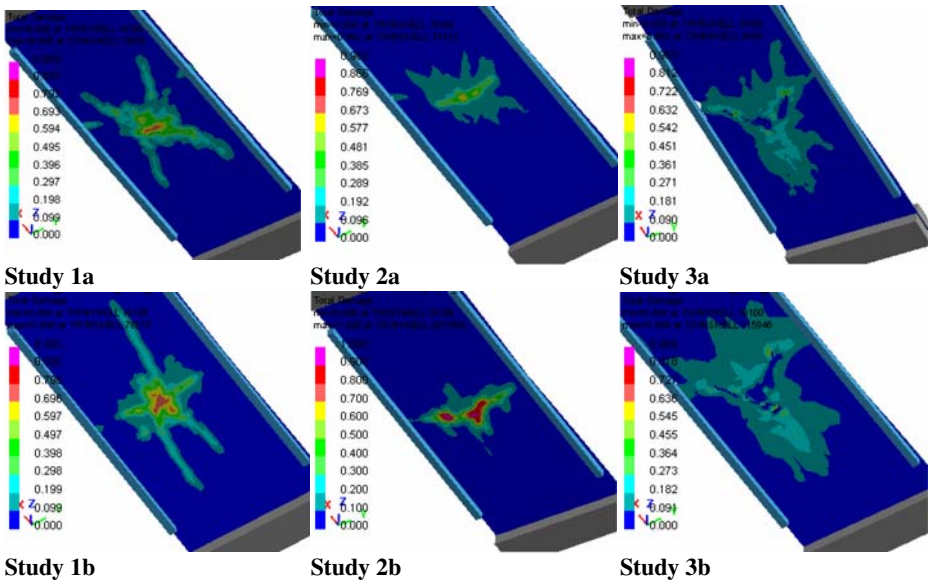

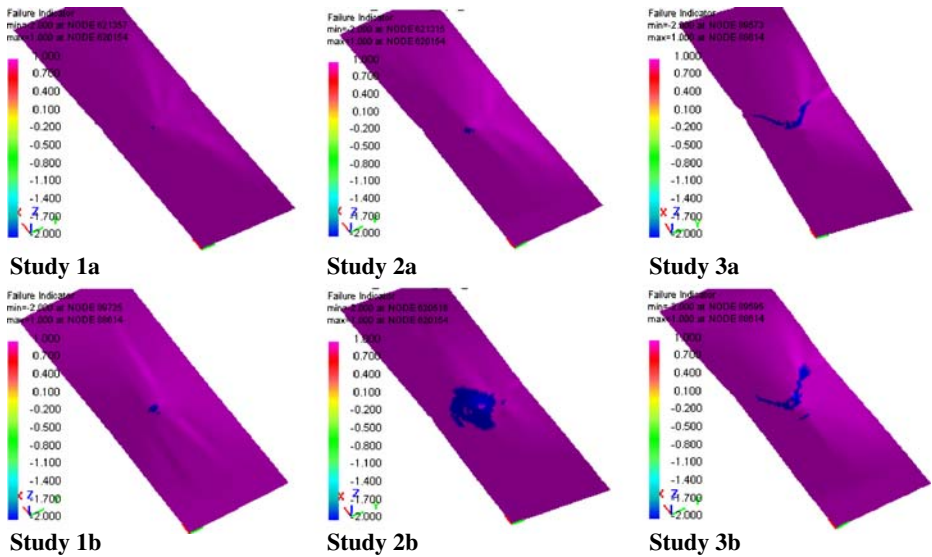**Fig. 11** Maximum ply damage on the lower ply (bottom view)

Fig. 12   Example of delamination damage between plies 3 and 4

in both ply and delamination damage if superimposed preloading is added. In the case of studies 2 and 3 the addition of preloading (studies 2b and 3b) has led to material failure which has not occurred in the case of the unloaded panels.

6.2.1 Studies 1a and 1b (Material T800S/M21 with QI Lay-Up)

The simulation force time histories for both studies, Fig. 13, show a good correlation with test measurements for both stiffness and maximum load. The preloaded panel does have a slightly lower, more distributed peak load, which appears to be due to the 'easier' creation of more dispersed material damage from the superimposed pre-loading. This is further seen in the contour plots of ply damage, Fig. 12, which shows a greater area of damage generated.
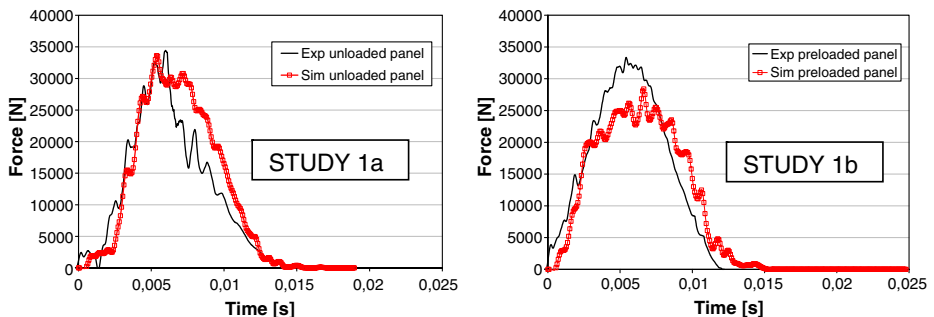

Fig. 13   Comparison of test and simulation impact force time histories for studies 1a and 1b
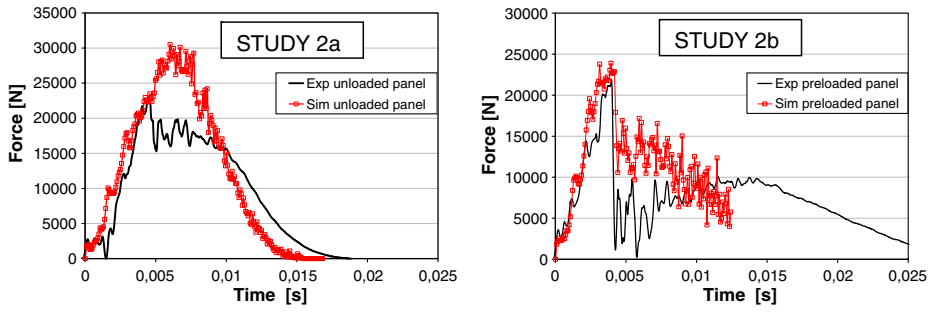
Fig. 14 Comparison of test and simulation impact force time histories for studies 2a and 2b
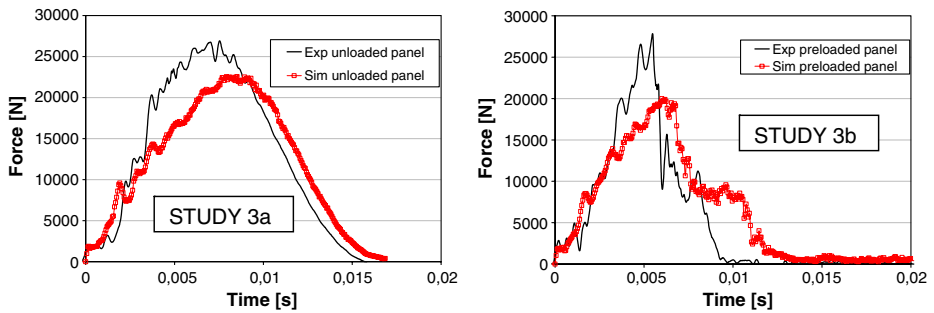

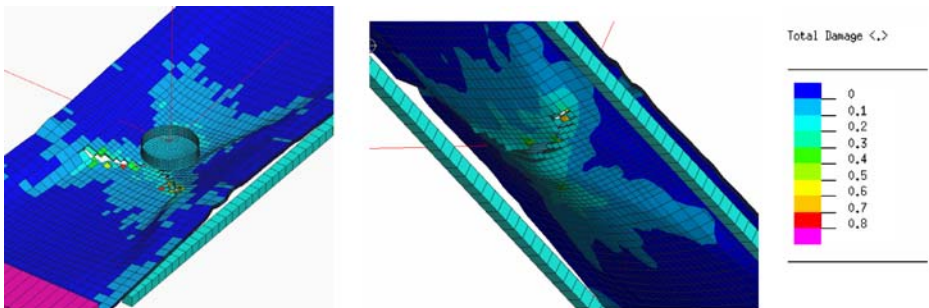Fig. 15 Comparison of test and simulation impact force time histories for studies 3a and 3b

Fig. 16 Maximum ply damage and shear failure for study 3b (preloaded)

6.2.2 Studies 2a and 2b (Material NCF/LY3505 with QI Lay-Up)

The simulation force time histories for these studies, Fig. 14, again show a good correlation for panel stiffness representation, although the prediction for maximum load in the unloaded case is over predicted. Failure modes for the pre-loaded case are well predicted, as is the post peak load decay seen in the impact force time history. Failure in this case is due to maximum load in the 0° plies being reached; this is clearly visible in Fig. 12 (study 2b). Contours of ply damage in the 0º direction, Fig. 10, also show the splitting modes that are to be found in the experimental results, Fig. 6.

6.2.3 Studies 3a and 3b (Material NCF/LY3505 with [±45]₁₆ Lay-Up)

The simulation force time histories for both studies, Fig. 15, show a less stiff loading response and under predict the maximum loads by 20–40%. This is not fully understood but may be due to material rate effects which are likely to be important for this matrix dominated intra-ply shear failure mode; the coupon and DCB specimens used to obtain material input and failure data were all conducted under quasi-static loading. The simulation does, however, correctly predict failure in the preloaded panel, although the ultimate failure modes, after maximum load, are different. In the test a punch through type failure occurs with large scale intra-ply shear failure, Fig. 7, whereas in the simulation shows failure to initiate under the punch which then propagates as a shear band toward the panel edges, Fig. 16.

7 Conclusions

A series of experimental and numerical simulations have been undertaken to investigate the effects of preloading on the damages processes that occur during impact loading of composites. Two composite materials; namely, a high performance aerospace UD pre-preg composite (T800S/M21) and lower performance biaxial NCF (NCF/LY3505) manufactured via liquid infusions methods have been investigated. This limited study has also considered different composite lay-ups including quasi-isotropic and ±45º.

The experimental studies have shown that pre-loading does significantly influence impact damage processes and, in two of the three cases investigated, also leads to earlier catastrophic failure of the composite. Simulation of the physical tests have shown an encouraging agreement with test results in terms of peak impact forces, the prediction of damage and the ability to correctly capture premature failure due to pre-loading. This would indicate that the proposed failure and delamination models used in this work have the ability to account for effects of pre-loading.

References

1. ASTM D7136, Standard test method for measuring the damage resistance of a fiber-reinforced polymer matrix composite to a drop-weight impact event, May 2005.
2. ASTM D7137, Standard test method for compressive residual strength properties of damaged polymer matrix composites, May 2005.
3. Whittingham, B., Marshall, I.H., Mitrevski, T., Jones, R.: The response of composite structures with pre-stress subject to low velocity impact damage. Composite Structures 66, 685–698 (2004)
4. Mikkor, K.M., Thomson, R.S., Herszberg, I., Weller, T., Mouritz, A.P.: Finite element modelling of impact on preloaded composite panels. Composite Structure 75, 501–513 (2006)

 5. PAM-CRASH™, ESI Software Engineering Systems International, 99 rue des Solets, SILIC 112, 94513 Rungis cedex France, 2006.
 6. Ladevèze, P., Le Dantec, E.: Damage modelling of the elementary ply for laminated composites. Composites Science and Technology **43**, 257–267 (1992)
 7. Greve L. and Pickett A.K., Modelling damage and failure in carbon/epoxy Non Crimp Fabric composites including effects of fabric pre-shear. Composites Part A, 37(11), pp 1983–2001, 2006.
 8. Pickett A. K. and Fouinneteau M. R. C., Material characterisation and calibration of a meso-mechanical damage model for braid reinforced composites, Composites: Part A, 37, pp 368–377, 2006.
 9. Fouinneteau M. R. C., Pickett A. K., Shear Mechanism modelling of heavy tow braided composites using a meso-mechanical damage model, Composites Part A, 2009.
10. Hillerborg, A., Modeer, M., Petersson, P.E.: Analysis of crack formation and crack growth in concrete by means of fracture mechanics and finite elements. Cement concrete Res **6**, 773–782 (1976)
11. Allix, O., Ladevèze, P.: Inter-laminar interface modelling for the prediction of laminates delamination. Composite structures **22**, 235–242 (1992)
12. Johnson, A.F., Pickett, A.K., Rozycki, P.: Computational methods for predicting impact damage in composite structures. Composites Science and Technology **61**, 2138–2192 (2001)
13. ISO international standard DIS15024. Fibre-reinforced plastic composites — Determination of Mode I interlaminar fracture toughness, GIC, for unidirectionally reinforced materials.
14. ASTM draft standard D30.06. Protocol for interlaminar fracture testing, End-Notched Flexure (ENF), revised April 24, 1993.
15. Reeder, J.R., Crews, J.H.: Mixed-mode bending method for delamination testing. AIAA Journal **28**(7), 1270–1276 (1989)
16. Greve L. and Pickett A. K., Delamination testing and modelling for composite crash simulation, Composites science and technology, 66, pp 816–826, 2006.
17. Grossir, S.: Mechanical Characterization and Simulation of Composite Impacts. MSc thesis, Cranfield University, UK (2004)